Human coronaviruses disassemble processing bodies

Carolyn-Ann Robinson[1*], Mariel Kleer[1*], Rory P. Mulloy[1,2*], Elizabeth L. Castle[3], Bre Q. Boudreau[4] and Jennifer A. Corcoran[1,4 #]

[1]Microbiology, Immunology and Infectious Diseases Department and Charbonneau Cancer Research Institute, University of Calgary, Calgary, AB, Canada.
[2]Department of Biochemistry, Microbiology and Immunology, University of Ottawa, Ottawa, ON, Canada.
[3] School of Biomedical Engineering, University of British Columbia, Vancouver, BC, Canada.
[4]Department of Microbiology and Immunology, Dalhousie University, Halifax, NS, Canada.
[*]Equal contribution
[#]Corresponding Author

Abstract

The *Coronaviridae* are a family of viruses with large RNA genomes. Seven coronaviruses (CoVs) have been shown to infect humans, including the recently emerged severe acute respiratory syndrome coronavirus 2 (SARS-CoV-2), the cause of coronavirus disease of 2019 (COVID-19). The host response to CoV infection is complex and regulated, in part, by intracellular antiviral signaling pathways triggered in the first cells that are infected. Emerging evidence suggests that CoVs hijack these antiviral responses to reshape the production of interferons and proinflammatory cytokines. Processing bodies (PBs) are membraneless ribonucleoprotein granules that mediate decay or translational suppression of cellular mRNAs; this is particularly relevant for proinflammatory cytokine mRNA which normally reside in PBs and are repressed. Emerging evidence also suggests that PBs or their components play important direct-acting antiviral roles, providing a compelling reason for their frequent disassembly by many viruses. No information is known about how human CoVs impact PBs. Here, we provide data to show that infection with the human CoV, OC43, causes PB disassembly. Moreover, we show that several SARS-CoV-2 gene products also mediate PB loss and virus-induced PB loss correlates with elevated levels of proinflammatory cytokine mRNAs that would normally be repressed in PBs. Finally, we demonstrate that stimulating PB formation prior to OC43 infection restricts viral replication. These data suggest that SARS-CoV-2 and other CoVs disassemble PBs during infection to support viral replication and evade innate immune responses. As an unintended side effect, the disassembly of PBs enhances translation of proinflammatory cytokine mRNAs which normally reside in PBs, thereby reshaping the subsequent immune response.

Introduction

PBs are ubiquitous, biomolecular condensates that form via liquid-liquid phase separation of proteins with regions of intrinsic disorder, and from RNA-protein and RNA-RNA interactions (1-5). PBs are comprised of the enzymes required for mRNA turnover, including those needed for decapping (Dcp2 and co-factors Dcp1a and Edc4/Hedls) and decay of the RNA body (5'-3' exonuclease Xrn1 and RNA helicase Rck/DDX6) and some components of the RNA-induced silencing complex (2,6). The RNA found in PBs consists of one third of all coding transcripts which are poorly translated and non-coding RNAs (2,4,7,8). mRNA transcripts, consisting predominantly of grouped regulatory mRNAs with related biological functions, are delivered to PBs by RNA-binding proteins (RBPs) (2,4). One such group bear destabilizing AU-rich elements (AREs) in their 3'-untranslated regions (3'-UTRs) and encode potent regulatory molecules like growth factors, pro-inflammatory cytokines, and angiogenic factors, making their turnover and/or suppression in PBs fundamental to our physiology (9-11). We and others showed that the presence of visible PBs correlates with increased turnover/suppression of ARE-mRNAs (11-15). Conversely, when PBs are lost, constitutive ARE-mRNA suppression is reversed. This provides cells with a means to rapidly respond to stimuli that disassemble PBs to produce proinflammatory cytokines, making PB disassembly an important yet underappreciated regulatory mechanism that tunes the production of potent proinflammatory cytokines that contain AREs, molecules like IL-6, IL-8, IL-1β, and TNF (9).

PBs are constitutive, dynamic ribonucleoprotein (RNP) granules that change in size and number in response to different stimuli. We and others have shown that stressors that activate the p38/MK2 MAP kinase pathway, as well as many virus infections elicit PB disassembly (12,13,15-18). Disassembly can occur by a direct interaction between a viral protein(s) and a PB component that is subsequently re-localized to viral replication and transcription compartments (vRTCs) (19-21) or cleaved by viral proteases (21-23). Viruses can also cause PB disassembly indirectly by activating p38/MK2 signaling (12,13). Despite numerous reports of viral gene products that trigger PB disassembly, corresponding reports of viral gene products that stimulate PB formation are rare, which suggests that PBs possess direct antiviral function and their disassembly may favour viral replication in ways that we fail to grasp (24). Even though other

RNPs such as stress granules have emerged as important components of our antiviral defenses that contribute to sensing virus and triggering innate immune responses (25-27), the evidence to support a direct antiviral role for PBs is less well established (24). A direct-acting antiviral role has been defined for several PB-localized enzymes that impede viral replication (e.g. APOBEC3G, MOV10). However, in these cases, the mechanism of viral restriction was attributed to the enzymatic activity of the PB protein(s) and its localization to PBs was not deemed as significant (20,21,23,28-35). PBs also harbour antiviral proteins that are important for innate immune signaling, diverting them and keeping them ready for the inducement of the desired antiviral response (20,36). It remains unclear if organization of particular proteins in PBs, or the higher order condensation of many proteins into the PB, regulates its antiviral activities. Nonetheless, the disassembly of PBs by diverse viruses strongly suggests their importance.

The family *Coronaviridae* includes seven viruses that infect humans, including the four circulating 'common cold' coronaviruses (CoVs), HCoV-OC43, HCoV-229E, HCoV-NL63, and HCoV-HKU1 and three zoonotic viruses that cause severe disease in humans: MERS-CoV, SARS-CoV, and the recently emerged SARS-CoV-2 (37,38). The latter is the infectious cause of coronavirus disease of 2019 (COVID-19). When severe, COVID is characterized by aberrant proinflammatory cytokine production, endothelial cell (EC) dysfunction and multiple organ involvement and has resulted in more than a million deaths worldwide thus far (39-44). Despite previous CoV epidemics, we do not yet appreciate precisely how SARS-CoV-2 infection causes the pathology observed in COVID and urgently need to define these molecular mechanisms to inform novel therapeutic strategies. Although all CoVs encode multiple proteins that hijack antiviral and interferon (IFN) responses (45), SARS-CoV-2 excels in this regard and a mismanaged IFN response is emerging as a major clinical determinant of COVID outcomes (45-48). In support of this, new evidence continues to reveal the multitude of mechanisms used by SARS-CoV-2 to out compete antiviral responses (49-53). For example, four SARS-CoV-2 non-structural proteins (nsp) were recently reported to each interact with specific cellular RNA targets to dramatically diminish IFN-β production and promote viral propagation (52).

To contribute to an enhanced understanding of how SARS-CoV-2 and other CoVs usurp cellular antiviral responses and alter cytokine mRNA expression profiles, we performed an analysis of

PBs. There is no published literature on human CoVs and PBs, and only two previous reports mentioned PB dynamics after CoV infection. Murine hepatitis virus (MHV) was reported to increase PBs at early infection times, while transmissible gastroenteritis coronavirus (TGEV) infected cells displayed complete PB loss by 16 hours post infection (24,54-56). We now present the first evidence to show that PBs are targeted for disassembly by a human CoV. We also show that SARS-CoV-2 encodes multiple proteins that when expressed alone are capable of causing PB loss, supporting a coordinated effort by CoVs to disassemble these granules. Finally, we show that prior formation of PBs restricts infection with OC43, delaying the expression of the viral nucleocapsid protein and preventing infectious progeny production. Taken together, these results suggest PBs play central role in the cellular antiviral responses to CoV infection.

Results

A screen of SARS-CoV-2 genes reveals mediators of PB loss

The genome of SARS-CoV-2 is predicted to contain up to 14 open reading frames (ORFs). The two N-terminal ORFs (1a and 1ab) encode two large polyproteins which are processed by viral proteases into 16 non-structural proteins (nsp1-16) essential for viral genome replication and transcription (37). The 3' end of the SARS-CoV-2 genome is predicted to code for ORFs that are expressed from 9 subgenomic mRNAs (57). Among these are the four structural proteins spike (S), envelope (E), membrane (M) and nucleocapsid (N) and up to 9 potential accessory proteins, not all of which have been validated in infected cells (37). To test the role of SARS-CoV-2 gene products in PB disassembly, we obtained a plasmid library of 27 SARS-CoV-2 genes from the Krogan lab; this library included 14 nsps (excluding nsp3 and nsp16), all structural (S, E, M, N) and candidate accessory genes (ORFs 3a, 3b, 6, 7a, 7b, 8, 9b, 9c, 10) and a catalytically inactive mutant version of the nsp5 3C-like protease (C145A) (57). We individually transfected each plasmid into HeLa cells that express a Dox-inducible GFP-tagged version of the PB-resident protein, Dcp1a (6). When fixed, these GFP-positive puncta co-stain with endogenous PB proteins such as the RNA helicase DDX6/Rck (Fig 1A) and the decapping co-factor hedls/Edc4 (Fig S1). While control cells or those transfected with the envelope (E) protein displayed DDX6-positive PBs, PBs were largely absent after transfection of six SARS-CoV-2 genes including the viral nucleocapsid (N) and the accessory gene, ORF7b (Fig 1A). We quantified number of DDX6-positive PBs per cell for each transfection using CellProfiler, as in (58). This quantification was performed in two different ways. In most cases, transfected cells were identified by co-staining for the Strep-tag II fused to each gene, as shown for N, E and ORF7b (Fig 1A). In such cases, we were able to count PBs only in cells with positive staining only and not count PBs in bystander cells (Fig 1B, thresholded). These data identified two SARS-CoV-2 proteins that may cause PB loss in a cell autonomous manner: ORF7b and N (Fig 1B). For the remaining transfections (nsp1, nsp5, nsp6, nsp11, nsp13, nsp14, ORF3b, ORF6, ORF9b, ORF9c) immunostaining for the Strep-tag II was not robust and we were unable to threshold our PB counts using CellProfiler. In these samples, we quantified PBs in all cells (Fig 1B, unthresholded). These data identified four additional SARS-CoV-2 proteins that may cause PB loss: ORF3b, nsp1, nsp6 and nsp11 (Fig 1B). We verified the expression of all constructs,

including low expressors (nsp1, nsp5, nsp6, nsp11, nsp13, nsp14, ORF3b, ORF6, ORF9b and ORF9c) by immunoblotting whole cell lysates harvested from parallel transfections (Fig 1C). We were unable to detect nsp4 and ORF10 by immunoblotting; however, we did visualize these proteins in immunostained samples. Consistent with previous work (57), we were unable to detect nsp6 by immunoblotting or by immunostaining, despite our observation that these cells appear to have less DDX6-positive puncta than our controls (Fig 1B, C).

A screen of SARS-CoV-2 genes reveals enhancers of an ARE-containing luciferase reporter

We performed a secondary reporter screen to identify SARS-CoV-2 proteins that enhanced the activity of a firefly luciferase (FLuc) reporter containing an ARE sequence in its 3' UTR, rendering the mRNA sensitive to constitutive turnover or translational suppression in PBs (59). For this reason, control samples display extremely low levels of FLuc luminescence relative to a non-ARE renilla luciferase (RLuc) transfection control, that reflects the turnover or suppression of the FLuc mRNA (Fig 2A). When reporter constructs are co-transfected with the positive control protein, KapB, which we have previously shown to cause PB disassembly and elevate the FLuc ARE-mRNA reporter (13,59), the relative luminescence is enhanced ~50-fold (Fig 2B). After co-transfection with the SARS-CoV-2 gene library, we identified three SARS-CoV-2 proteins that significantly elevated relative luminescence as well as or better than KapB: nsp1 (150-fold), nsp14 (80-fold), and ORF7b (40-fold), and two others that elevated luminescence 10-20-fold: nsp13 and ORF6 (Fig 2B). Of these ARE-mRNA regulating SARS-CoV-2 gene products, two overlap with those we showed to cause PB loss, nsp1 and ORF7b (Fig 1).

Validation of SARS-CoV-2 genes that cause PB loss in primary endothelial cells

Endothelial cells (ECs) have emerged as playing a significant role in severe COVID, they are also sources for many of the cytokines elevated in severe disease and are infected by SARS-CoV-2 (48,60-63). We validated top hits from our PB and ARE-containing reporter screen in human umbilical vein endothelial cells (HUVECs) that were transduced with recombinant lentiviruses expressing N, nsp14 or a vector control. Transduced cells were selected and stained for the endogenous PB marker protein DDX6 and for the Strep-tag II on each of SARS-CoV-2 constructs. Compared to the control, we observed PB loss in N-expressing cells and a decrease in PB numbers in the nsp14-transduced cell population (Fig 3). We also observed that in some

cells, nsp14 staining, although usually difficult to detect, overlapped with DDX6-positive puncta in nsp14-transfected HeLa cells (Fig 3B, C). The significance of this observation is unclear and we are investigating it further.

Infection of endothelial cells with human coronavirus causes PB loss

To understand if PBs were lost during infection with human coronaviruses, we established an infection model for the human CoV, OC43, in HUVECs. We tested the ability of OC43 to enter and replicate in these primary cells and confirmed that HUVECs are permissive to OC43 (Fig 4A). We then performed a time-course experiment wherein OC43-infected HUVECs were fixed at various times post infection and stained for DDX6 (PBs) and the viral nucleocapsid (N) protein to denote infected cells. We observed that PBs were lost after infection with OC43 but not lost over the time course of the experiment in our mock-infected control cells (Fig 4A-B). These results showed that PB counts were significantly diminished at 12 and 24 hpi (Fig 4A-B). To determine if the reduced PB counts correlated with changes to cytokine mRNA levels, we harvested total RNA from OC43-infected cells at 24 hpi and performed RT-qPCR for two ARE-containing cytokine transcripts, IL-6 and IL-8 (Fig 4C). Consistent with the observed reduction in PBs, the steady-state levels of IL-6 and IL-8 mRNA both increased ~20-fold compared to uninfected cells (Fig 4C). We also observed, in some infected cells, DDX6-positive puncta reappeared at 24 hpi, but these puncta did not resemble PBs in terms of their size or shape but were larger, non-spherical aggregates. It is unclear at this time if these DDX6-positive aggregates represent vRTCs or stress granules, another RNP granule that viruses manipulate (25,26). Further experiments will determine the nature of these aggregates.

PBs restrict coronavirus infection

Since SARS-CoV-2 encodes six proteins that induce PB loss and infection with OC43 recapitulates this loss, we hypothesized that PBs may be able to restrict coronavirus infection. To test this, we used lentiviruses to deliver the fluorescently-labeled PB protein, GFP-Dcp1a, or a control GFP protein to HUVECs prior to infecting with OC43. At various times post infection, cells were fixed and stained for the viral nucleocapsid (N) protein (Fig 5A). Although OC43 was able to express N in GFP-positive control cells, we observed viral N gene expression was restricted in cells that expressed GFP-Dcp1a (Fig 5A). The restriction was most pronounced at

6hpi, when we observed only ~20% of GFP-Dcp1a-positive cells were visibly infected, compared to the GFP-only controls (Fig 5B). At later infection times, more N gene expression was observed in cells also expressing GFP-Dcp1a, suggesting that OC43 infection was able to overcome the restriction imposed by GFP-Dcp1a (Fig 5B). Next, we examined if an increased dose of the GFP-Dcp1a lentivirus, that should elicit the formation of more PBs, would increase the restrictive phenotype (Fig 5C). HUVECs were transduced with 5-fold more GFP-Dcp1a lentivirus than in Fig 5B, infected with OC43, and the infected cell supernatant was collected at 24hpi (Fig 5C). The amount of OC43 infectious particles produced in each condition was determined using a TCID50 assay (64). Infectious OC43 particles were produced from control cell populations transduced with the GFP virus and there was no significant difference in viral particles produced after transduction with a lower dose of GFP-Dcp1a lentivirus (Fig 5C). However, the addition of 5-fold more GFP-Dcp1a lentivirus prior to OC43 infection restricted viral replication and no infectious OC43 particles were detected in the 24hpi-supernatant taken from these cells (Fig 5C). Taken together, these data show that PB fortification prior to OC43 virus infection restricts virus replication, providing a compelling reason why SARS-CoV-2 would coordinate an attack on cellular PBs using multiple viral proteins.

Discussion

In this manuscript, we present data to show that the human CoV, OC43, causes PB loss during infection. The loss of PBs correlates with elevated steady-state levels of two PB-regulated cytokines, IL-6 and IL-8. Using a gene library, we also identify six candidate gene products encoded by SARS-CoV-2 that are capable of inducing PB loss and three candidate gene products that stabilize an ARE-containing luciferase reporter. Moreover, we present evidence that prior fortification of PB granules using overexpression of the PB protein, GFP-Dcp1a, restricts the infectious cycle of OC43, delaying viral nucleocapsid protein production and preventing infectious progeny production. These data support our model that PBs are antiviral granules designed to protect cells from viral invaders.

Multiple SARS-CoV-2 gene products highlight the diversity of approaches used by one virus to induce PB loss

We screened 27 SARS-CoV-2 gene products by transfection in HeLa cells (57) and identified six candidates that reduce PB numbers including the viral nucleocapsid protein (N), the viral host shutoff factor (nsp1), non-structural proteins nsp6 and nsp11, and accessory proteins ORF7b and ORF3b (Fig 1). The most significant of these candidates was the N protein, which we also showed caused endogenous PB loss in primary ECs (Fig 3). N is a multifunctional RNA-binding protein (RBP) that coats the viral genome and induces phase separation to promote viral particle assembly (37,65-68). N possesses several non-specific RNA-binding regions and is phosphorylated in its central serine-arginine (SR-rich) domain (68,69). SARS-CoV-2 N also contains three putative NLS sequences (70). One possible reason for PB loss may be the indiscriminate RNA binding of N protein which acts as sponge for RNA, pulling it out of cytoplasm, reducing the RNA-protein interactions required for phase separation of PBs (3). We are currently engaged in site-directed and truncation mutagenesis studies to determine the precise region(s) of N that are essential for its effect on PBs (71). Another PB-regulating SARS-CoV-2 protein we discovered is the bifunctional enzyme, nsp14, which possesses an N-terminal exonuclease domain (ExoN) required for proofreading of the CoV polymerase complex and a C-terminal N-methyltransferase (MTase) domain that contributes to viral RNA capping (37,72). Nsp14 caused PB loss in our EC validation studies yet it did not cause PB loss in HeLa cells (Fig 1, 3). Though we are unclear of the precise reason for these discrepant results, one consideration

is that GFP-Dcp1a expression in HeLa cells makes PBs more stable and their disassembly more difficult. It was also quite difficult to detect the expression of nsp14 in HeLa cells after their transfection, although nsp14 was detected by immunoblotting; therefore, PBs were counted in all cells, and the results were not specific for cells that expressed nsp14 (Fig 1). In contrast, in our EC validation studies we selected for transduced cells; thus, all ECs contain nsp14 even if the staining is low (Fig 3). This may explain the significant PB loss observed in ECs and not in HeLa cells. Finally, we observed that nsp14 occasionally formed small puncta that overlapped with DDX6-positive PBs in both HeLa cells and ECs (Fig 3A, 3C). There are no previous reports of any other CoV proteins co-localizing to PBs. The significance of this observation remains unclear. We will continue to interrogate nsp14 localization using confocal microscopy and immunoprecipitation assays. Nsp14 was also a significant hit in the luciferase reporter assay (Fig 2), suggesting that nsp14 promotes the stabilization or translation of PB-localized, ARE-containing cytokine mRNA. Consistent with this, alphacoronavirus nsp14 enhanced TNF and IFN-β (both these mRNAs contain AREs) independent of its enzymatic functions, a phenotype that is consistent with a PB-regulating protein (73).

Our initial validation efforts have focused on nsp14 and N (Fig 3); however, our screens did highlight other SARS-CoV-2 proteins that may regulate PBs to enhance translation of ARE-mRNAs. These include the top hit in our luciferase screen, nsp1. All CoVs encode a host shutoff protein called nsp1 that is the first protein expressed after virus entry and an important IFN antagonist that limits IFN and interferon-stimulated gene translation (52,74). SARS-CoV-2 nsp1 binds to 18S rRNA and the blocks the mRNA entry channel in the 40S ribosomal subunit, thereby blocking translation (52,75). Given its role in translation shutoff and RNA decay, we were initially concerned that nsp1-mediated elevation in the ARE-containing FLuc reporter was non-specific because we observed low levels of the RLuc control that could suggest global translation shutoff (52,76-78). However, stress-responsive cellular transcripts are often resistant to the action of nsp1and other viral shutoff proteins suggesting that the sequestration of regulatory transcripts in PBs is a strategy used by cells to withstand viral host shutoff (74,77,79). For this reason, PB-regulated transcripts like the ARE-containing FLuc reporter may be resistant to nsp1-mediated shutoff (Fig 2). We are currently validating if nsp1 is a PB-regulating viral protein in ECs and will explore its effects on cytokine mRNA levels. In addition, ORF7b and the

short ORF3b are intriguing hits because both are accessory proteins that have been reported to either activate the kinase p38 (an inducer of PB disassembly) or antagonize IFN responses (53,80). Not picked up in our screen, the viral 3C-like protease, nsp5, is also of particular interest because porcine CoV nsp5 cleaves Dcp1a, an event that would be predicted to cause PB disassembly (81). Although nsp6 and nsp11 were top hits in our unthresholded PB screen (Fig 1), their expression is either toxic or difficult to detect and we are engaged in developing strategies to minimize these issues and study them further.

PBs are antiviral granules that restrict CoV infection

We used the human CoV, OC43, to infect ECs and show that virus infection caused significant PB loss at 12 and 24 hpi (Fig 4). We then fortified PBs using the overexpression of GFP-Dcp1a and showed that PB fortification before infection delayed the visual expression of viral nucleoprotein and restricted the production of infectious viral particles (Fig 5). However, the precise details of the mechanism of restriction remain unclear. We are engaged in ongoing time course experiments to determine if the restrictive phenotype represents a delay of viral progeny production or a complete block. It is also unclear if the prior GFP-Dcp1a overexpression restricts OC43 replication due to a direct antiviral role of the Dcp1a enzyme itself or its ability to promote the formation of larger PBs (82,83). GFP-Dcp1a overexpression is a common approach used to visualize PBs, and we know these GFP-positive puncta co-stain with endogenous PB proteins (Fig 1) (82). However, GFP-Dcp1a puncta are larger and may be more stable than endogenous PBs (56,83). Our ongoing work will utilize other molecular tools that regulate PB dynamics to determine if certain PB resident proteins exert antiviral properties independent from the formation of the PB granule itself. We are currently engaged in experiments to overexpress different PB proteins that have roles in RNA decay (Dcp1a, DDX6 RNA helicase, the decapping cofactor hedls/Edc4 or the exonuclease Xrn1) as well as PB proteins that do not directly mediate RNA decay but play an important condensation role for PB granule formation (Lsm14A, 4E-T) (3,4,84). Each of the proposed proteins will affect PBs differently when overexpressed: Dcp1a, hedls/Edc4 and DDX6 increase PB formation, with Dcp1a expression inducing larger granules than the others, Dcp2 has no effect on granule size/number, and Xrn-1 eliminates PBs because it increases mRNA decay (4,83-86). We predict that other GFP-tagged PB proteins that promote molecular condensation of PBs, such as GFP-DDX6, will also restrict OC43 infection.

Conversely, we expect that the overexpression of Xrn1 will promote viral infection (as shown by others (34)) because it prevents PB formation, even though it can degrade viral RNA.

There is increasing evidence in support of our hypothesis that the antiviral role of PB-localized enzymes is promoted by phase separation of molecules into PBs and that the antiviral function of these molecules is lost when PB granules decondense. This has been previously proposed for decapping complexes, the enzymatic activity of which is increased by phase separation and decreased in solution (3-5). However, for PB-localized enzymes that have established antiviral effects, (e.g. APOBEC, MOV10), their ability to restrict virus infection has previously been attributed to their enzymatic activity rather than their localization to PBs (20,21,23,29-35,82). Therefore, it is not yet clear if the antiviral capability of PBs relies on their formation into biomolecular condensates. Here, we consider that the antiviral restriction promoted by PB-localized enzymes requires the granule formation for optimal function. By that definition, factors that promote PB condensation may also be antiviral. Therefore, in part one of our model, we propose that PBs are direct-acting antiviral granules that can restrict virus infection when present as visible condensates; for this reason, they are targeted by disassembly by most viruses.

PBs interact with other innate immune pathways to regulate antiviral signaling

One possibility is that PBs are antiviral because their proteins help the cell respond to signals that activate innate immune pathways (20,22,36,85). It is not clear if PB antiviral activities are connected to established regulators of innate immune signaling such as the RNA sensors RIG-I/MDA5, transcription factors IRF3/NF-kB, or the production of Type I IFNs, though reports suggest this may indeed be the case (36,85,87). The recent demonstration that TRAF6 controls Dcp1a localization within PBs using ubiquitylation suggests that antiviral signaling is more complex than previously appreciated and integrates transcriptional responses with cytokine mRNA suppression in PBs (85,87). Moreover, the PB protein Lsm14A has also been shown to bind to viral RNA/DNA after infection to promote IRF3 activation and IFN-β production (36). Although it remains unclear if organization of particular proteins in PBs, or the higher order condensation of many proteins into the PB, regulates its antiviral activity (82,87), what is clear is that PB disassembly reverses the constitutive decay or translational suppression of cytokine mRNAs that contain AREs that would normally occur there (11-15,88). These data suggest that

when viruses coordinate an attack to cause PB loss, this event relieves the cytokine mRNA suppression and acts as a danger signal that signals the immune system for help. In this way, PB disassembly may be a central component of the cellular innate immune response and part of the sequelae of signals that notify the immune system that a cell is infected. In situations where interferon responses are delayed or defective, as is emerging for SARS-CoV-2 and severe COVID (45-53), PB disassembly may be an important contributing factor to pathogenic cytokine responses. Therefore, in part two of our model, we propose that cells view viral PB disassembly as a danger signal and respond by increasing production of proinflammatory cytokines as a call for reinforcements.

A new model for the role of PBs as a nexus of intracellular antiviral responses

We now propose a model for how PBs may regulate cellular innate responses to CoV infection (Fig 6). Our model places PBs at a nexus point, a connection between intracellular direct-acting antiviral responses and proinflammatory cytokine responses. We propose that PBs function as direct-acting antiviral granules that can restrict virus infection if robustly induced into phase-separated molecular condensates; for this reason, they are targeted by disassembly by most viruses. Second, when viral invaders cause PB loss, the cell responds to the inactivation of PBs with a call for reinforcements. This occurs because PBs house suppressed cytokine transcripts which are relieved of their suppression by viral PB disassembly. This model places the PB as a central player in the antiviral response that coordinates the immune reshaping that occurs after CoV infection.

Materials and Methods

Cell culture

All cells were maintained at 37 °C with 5% CO_2 and 20% O_2. Vero E6 (ATCC), HEK293T cells (ATCC), HeLa Tet-Off cells (Clontech) and HeLa Flp-In TREx GFP-Dcp1a cells (a generous gift from Anne-Claude Gingras (6)) were cultured in DMEM (Thermo Fisher) supplemented with 100 U/mL penicillin, 100 µg/mL streptomycin, 2 mM L-glutamine (Thermo Fisher) and 10% FBS (Thermo Fisher). HUVECs (Lonza) were cultured in endothelial cell growth medium (EGM-2) (Lonza). HUVECs were seeded onto gelatin-coated tissue culture plates or glass coverslips.

Plasmids and Cloning

pLenti-IRES-Puro SARS-CoV2 plasmids were a generous gift from the Krogan Lab (89). pLJM1-GFP-Dcp1a was generated by cloning pT7-EGFP-C1-HsDCP1a (Addgene 25030) into pLJM1-BSD (90)using AgeI and SmaI restriction sites (NEB). pLJM1-KapB-BSD was generated by cloning pBMNIP-KapB (13) into pLJM1-BSD using EcoRI and BamHI restriction sites (NEB).

Transient Transfections

Transient transfections were performed using Fugene (Promega) according to manufacturer's guidelines. Briefly, HeLa Flp-In TREx GFP-Dcp1a cells were seeded in 12-well plates at 150,000 cells/well in antibiotic-free DMEM on coverslips for immunofluorescence or directly in wells for lysates. Cells were transfected with 1 µg of DNA and 3 µL of Fugene for 48 h before processing.

Lentivirus generation

All lentiviruses were generated using a second-generation system. Briefly, HEK293T cells were transfected with pSPAX2, MD2G, and the plasmid containing a gene of interest using polyethylimine (PEI, Polysciences). Viral supernatants were harvested 48 h post-transfection and frozen at -80°C until use. For transduction, lentiviruses were thawed at 37°C and added to target cells in complete media containing 5 µg/mL polybrene (Sigma) for 24 h. The media was changed to selection media containing 1 µg/mL puromycin or 5 µg/mL blasticidin (Thermo Fisher) and cells were selected for 48 hours before proceeding with experiments.

Immunofluorescence

Cells were seeded onto coverslips for immunofluorescence experiments. Following treatment, cells were fixed for 10 mins at 37 °C in 4% (v/v) paraformaldehyde (Electron Microscopy Sciences). Samples were permeabilized with 0.1% (v/v) Triton X-100 (Sigma-Aldrich) for 10 min at room temperature and blocked in 1% human AB serum (Sigma-Aldrich) 1 h at room temperature. Primary and secondary antibodies were diluted in 1% human AB serum and used at the concentrations in Table 1. Nuclei were stained with DAPI. Samples were mounted with Prolong Gold AntiFade mounting media (Thermo).

Immunoblotting

Cells were lysed in 2X Laemmli buffer and stored at -20°C until use. The DC Protein Assay (Bio-Rad) was used to quantify protein concentration as per the manufacturer's instructions. 10-15 µg of protein lysate was resolved by SDS-PAGE on 4-15% gradient TGX Stain-Free acrylamide gels (BioRad). Total protein images were acquired from the PVDF membranes after transfer on the ChemiDoc Touch Imaging system (BioRad). Membranes were blocked in 5% BSA in TBS-T. Primary and secondary antibodies were diluted in 2.5% BSA, and used at the dilutions found in Table 1. Membranes were visualized using Clarity Western ECL substrate and the ChemiDoc Touch Imaging system (BioRad).

Luciferase Assays

HeLa Tet-Off cells were transfected according to Corcoran J.A. et al. *Methods* (2011) with pTRE2-Firefly Luciferase-ARE, pTRE2-Renilla Luciferase, and SARS-CoV2 plasmids using Fugene HD (Promega). Firefly and Renilla luciferase activity were quantified using the Dual Luciferase Assay Kit (Promega) and read on a Modulus Microplate luminometer (Promega).

Quantitative PCR

RNA was collected using an RNeasy Plus Mini Kit (Qiagen) according to the manufacturer's instructions and stored at -80°C until use. RNA concentration was determined and was reverse transcribed using qScript XLT cDNA SuperMix (QuantaBio) using a combination of random hexamer and oligo dT primers, according to the manufacturer's instructions. Depending on starting concentration, cDNA was diluted between 1:10 and 1:20 for qPCR experiments and SsoFast EvaGreen Mastermix (Biorad) was used to amplify cDNA. The ΔΔquantitation cycle (Cq) method was used to determine the fold change in expression of target transcripts. qPCR primer sequences can be found in Table 2

OC43-CoV Propagation and Infection

Stocks of hCoV-OC43 (ATCC) were propagated in Vero E6 cells. To produce viral stocks, Vero E6 cells were infected at an MOI of 0.01 for 1 h in serum-free DMEM at 33˚C. Following infection, the viral inoculum was removed and replaced with DMEM supplemented with 2% heat-inactivated FBS and 100 units/mL penicillin/streptomycin/glutamine. After 6 days, the supernatant was harvested and centrifuged at 2000 RPM for 5 mins to remove cellular debris. Virus stocks were aliquoted and stored at -80˚C for single use. Viral titers were enumerated using Reed and Muench tissue-culture infectious dose 50% (TCID50) in Vero E6 cells (64). For infection, cells were seeded onto coverslips to achieve ~70% confluency after 24 hours. The following day, the growth media was removed and replaced with 100 µl of human CoV-OC43 inoculum and incubated at 37˚C for one hour, rocking the plate every 10 minutes to distribute viral inoculum. Following incubation, the virus inoculum was removed and replaced with EGM-2.

Processing Body Quantification

Processing bodies were quantified using an unbiased image analysis pipeline generated in the freeware CellProfiler (cellprofiler.org) (91). First, detection of nuclei in the DAPI channel image was performed by applying a binary threshold and executing primary object detection between 50 and 250 pixels. From each identified nuclear object, the “Propagation” function was performed on the respective CoV2-ORF channel image to define cell borders. The identified cell borders were masked with the identified nuclei to define a cytoplasm mask. The cytoplasm mask was then applied to the processing body puncta channel image to ensure only cytoplasmic puncta were quantified. Background staining was reduced in the cytoplasmic puncta channel using the “Enhance Speckles” function. Using “global thresholding with robust background adjustments”, puncta within a defined size and intensity range were quantified. Size and intensity thresholds were unchanged between experiments with identical staining parameters. Intensity measurements of puncta and CoV2-ORF staining were quantified. Quantification data was exported and RStudio was used for data analysis.

Statistics

All statistical analyses were performed using GraphPad Prism 8.0. Significance was determined using the tests indicated in each of the figure legends.

Figure Legends

Figure 1: A screen of SARS-CoV2 genes reveals mediators of processing body loss. A: HeLa Flp-In TREx GFP-Dcp1a cells were transfected with an empty vector or 2xStrep-tagged SARS-CoV2 ORFs for 48 h and then fixed and immunostained for Strep-tag (red), DDX6 (white), and nuclei (blue). Select ORFs are shown; Scale bar=20 μm. B: DDX6 puncta were quantified using CellProfiler on SARS-CoV2 ORF-expressing cells thresholded by Strep-tag staining intensity. The intensity threshold used to determine ORF-expressing cells was defined as two standard deviations above mean intensity in vector controls. Values are expressed as a fold-change difference normalized to the vector control (hashed line). A one-way ANOVA with a Dunnett's post-hoc analysis was performed, n=3; bars represent SEM; **=P<0.01. C: Lysates were harvested from HeLas transfected with 2xStrep-tagged SARS-CoV2 ORFs after 48 h of expression in 2x Laemmli buffer. Samples were resolved by SDS-PAGE on 4-15% gradient gels (BioRad) and immunoblotted with a Strep-Tag II antibody (Sigma).

Figure 2: ARE-mRNA stability is affected by SARS-CoV2 gene expression. A: Schematic of luciferase constructs used for ARE-mRNA stability assay. Both firefly and renilla luciferase are under the control of a promoter that is inhibited in the presence of doxycycline. The firefly luciferase construct contains an AU-rich element (ARE) in its 3' UTR, targeting it for degradation in the presence of processing bodies. B: HeLa Tet-Off cells were transfected with both the firefly (FLuc) and renilla (RLuc) luciferase constructs with either an empty vector, kaposin B (KapB, positive control), or the SARS-CoV2 genes. Doxycycline was added 36 h post-transfection to stop expression of luciferase constructs from TRE2 promoters and cells were lysed at 48 h post-transfection. Firefly and renilla luminescence were measured using a Dual Luciferase Reporter Assay System (Promega) and a Modulus Microplate (Promega). Values are reported as firefly luminescence/renilla luminescence normalized to the empty vector control. A one-way ANOVA with a Dunnett's post-hoc analysis was performed, n=3; bars represent SEM; ****=P<0.0001; # nsp1 caused low renilla luciferase values resulting in an artificially high firefly/renilla value.

Figure 3: SARS-CoV2 genes induce processing body disassembly in primary endothelial cells. A: Human umbilical vein endothelial cells (HUVECs) were transduced with selected 2xStrep-

tagged SARS-CoV2 ORFs or an empty vector control and selected with puromycin for 48 h. Samples were fixed and immunostained for Strep-tag (red), DDX6 (white), and nuclei (blue). Scale bar=20 μm. B: DDX6 puncta were quantified using CellProfiler on the images in A. Values are expressed as a fold-change difference normalized to the empty vector control (hashed line). n=2, bars indicate ranges. C: HeLa Flp-In TREx GFP-Dcp1a cells were transfected with SARS-CoV2 nsp14 and fixed 48 h post-transfection. Samples were immunostained for Strep-tag (white) and DDX6 (red). White arrows indicate overlapping staining.

Figure 4: Human coronavirus OC43 disassembles processing bodies in primary endothelial cells. A: HUVECs were infected with OC43 (viral stock of $3.5x10^4$ TCID50/mL). Samples were fixed at the indicated times post-infection and stained for OC43-N protein (green), DDX6 (white), and nuclei (blue). Scale bar=20 μm. B: Using images from A, DDX6 puncta in mock or OC43 infected cells were quantified using CellProfiler. Values are represented as fold-change relative to mock (hashed line). A one-way ANOVA with a Dunnett's post-hoc analysis was performed, n=3; bars represent SEM; *=$P<0.05$. C: RT-qPCR was performed for ARE-mRNAs, IL-6 and IL-8, on OC43 infected HUVECs at 24 hpi. n=3; bars represent geometric SD.

Figure 5: Overexpression of GFP-Dcp1a restricts OC43 infection. A: HUVECs were transduced with lentiviruses expressing either a GFP-control or GFP-Dcp1a prior to being infected with OC43 (with a viral stock of $3.5x10^4$ TCID50/mL). Samples were fixed at 6, 12, and 24 hpi (only 6 and 24 hpi shown) and stained for OC43-N protein (red) and nuclei (blue). Scale bar=20 μm. B: Using images from A, infected and uninfected cells were quantified at 6, 12, and 24 hpi. Values are represented as fold-change relative to the paired GFP control for each time point. For 6 hpi, n=2; for 12 and 24 hpi n=3. C: Supernatants were harvested at 24 hpi and titrated on naive Vero E6 cells using TCID50. n=2.

Figure 6: Processing bodies are a nexus point for virus-host conflict. In part one of our model, we hypothesize that PBs are direct-acting antiviral granules that can restrict virus infection when present as visible condensates; for this reason, they are targeted for disassembly by most viruses. In part two of our model, we propose that viral PB disassembly is perceived by the cell as a danger signal and relieves suppressed cytokine transcripts to produce proinflammatory cytokines

that recruit and activate immune cells. In this way, PB disassembly may also contribute to the pathogenic cytokine responses that underly many viral illnesses including COVID.

Figure S1: Hedls/Edc4 staining colocalizes with GFP-Dcp1a puncta to visualize processing bodies. HeLa Flp-In TREx GFP-Dcp1a cells were induced with 1 μg/mL doxycycline for 24 h. Samples were fixed and immunostained for the PB resident protein Hedls/Edc4 (red). Scale bar=20 μm.

Table 1: Antibodies

Antibody	Species	Vendor/Catalog #	Application	Dilution
Strep-Tag II	Mouse	Sigma (71590-M)	Immunofluorescence Immunoblot	1:1000 1:1000
DDX6	Rabbit	Bethyl (A300-461)	Immunofluorescence	1:1000
Coronavirus OC43	Mouse	Millipore (MAB9012)	Immunofluorescence	1:500
Alexa Fluor 555-donkey anti-mouse	Donkey	Thermo Fisher (A31570)	Immunofluorescence Secondary	1:1000
Alexa Fluor 555-donkey anti-rabbit	Donkey	Thermo Fisher (A31572)	Immunofluorescence Secondary	1:1000
Alexa Fluor 488-chicken anti-mouse	Chicken	Thermo Fisher (A21200)	Immunofluorescence Secondary	1:1000
Alexa Fluor 488-chicken anti-rabbit	Chicken	Thermo Fisher (A21441)	Immunofluorescence Secondary	1:1000
Alexa Fluor 647-chicken anti-mouse	Chicken	Thermo Fisher (A21463)	Immunofluorescence Secondary	1:1000

Table 2: RT-qPCR primers

Target	Direction	Sequence 5'-3'
HPRT	Forward	CTTTCCTTGGTCAGGCAGTATAA
HPRT	Reverse	AGTCTGGCTTATATCCAACACTTC
18S	Forward	TTCGAACGTCTGCCCTATCAA
18S	Reverse	GATGTGGTAGCCGTTTCTCAGG
B2M	Forward	TTTCCATTCTCTGCTGGATGAC
B2M	Reverse	TGCTGTCTCCATGTTTGATGTA
IL6	Forward	GTCCAGTTGCCTTCTCCCTGG
IL6	Reverse	GAGATGCCGTCGAGGATGTACC
CXCL8	Forward	AAATCTGGCAACCCTAGTCTG
CXCL8	Reverse	GTGAGGTAAGATGGTGGCTAAT
IL-1β	Forward	CTCTCACCTCTCCTACTCACTT
IL-1β	Reverse	TCAGAATGTGGGAGCGAATG
TNF	Forward	TCGAACCCCGAGTGACAA
TNF	Reverse	AGCTGCCCCTCAGCTTG
GM-CSF	Forward	AAATGTTTGACCTCCAGGAGCC
GM-CSF	Reverse	ATCTGGGTTGCACAGGAAGTT
COX-2	Forward	CCCTTGGGTGTCAAAGGTAA
COX-2	Reverse	GCCCTCGCTTATGATCTGTC
VEGF	Forward	CGAGACCTTGGTGGACATC
VEGF	Reverse	CTGCATGGTGACGTTGAAC

530 Table 3: Plasmids

Plasmid Name	**Use**	**Source**	**Mammalian Selection**
pLJM1-BSD	Empty vector control	(90)	Blasticidin
pLJM1-KapB-BSD	Positive control	Cloned from pBMNIP-KapB (13) into pLJM1-BSD	Blasticidin
pLJM1-GFP-DCP1a-BSD	Overexpression	Cloned from pT7-EGFP-C1-HsDCP1a (Addgene 25030) into pLJM1-BSD	Blasticidin
pLenti-SARS-CoV2-IRES-Puro	Overexpression library	(89)	Puromycin
pTwist-SARS-CoV2-Spike-IRES-Puro	Overexpression	(89)	Puromycin
pTRE2-Firefly Luciferase-ARE	ARE-mRNA stability	(59)	N/A
pTRE2-Renilla Luciferase	ARE-mRNA stability	(59)	N/A
pMD2.G	Lentivirus generation	Addgene 12259	N/A
psPAX2	Lentivirus generation	Addgene 12260	N/A

531
532
533
534

References

1. Cougot N, Cavalier A, Thomas D, Gillet R. The dual organization of P-bodies revealed by immunoelectron microscopy and electron tomography. J Mol Biol. 2012 Jun 29;420(1-2):17–28.

2. Hubstenberger A, Courel M, Bénard M, Souquere S, Ernoult-Lange M, Chouaib R, et al. P-Body Purification Reveals the Condensation of Repressed mRNA Regulons. Mol Cell. Elsevier Inc; 2017 Oct 5;68(1):144–5.

3. Corbet GA, Parker R. RNP Granule Formation: Lessons from P-Bodies and Stress Granules. Cold Spring Harb Symp Quant Biol. 2019;84:203–15.

4. Riggs CL, Kedersha N, Ivanov P, Anderson P. Mammalian stress granules and P bodies at a glance. J Cell Sci. 2020 Sep 1;133(16):jcs242487.

5. Tibble RW, Depaix A, Kowalska J, Jemielity J, Gross JD. Biomolecular condensates amplify mRNA decapping by coupling protein interactions with conformational changes in Dcp1/Dcp2. 2020 Jul 9;60th Anniversary(479–480):600–36.

6. Youn J-Y, Dunham WH, Hong SJ, Knight JDR, Bashkurov M, Chen GI, et al. High-Density Proximity Mapping Reveals the Subcellular Organization of mRNA-Associated Granules and Bodies. Mol Cell. 2018 Feb 1;69(3):517–532.e11.

7. Khong A, Parker R. mRNP architecture in translating and stress conditions reveals an ordered pathway of mRNP compaction. J Cell Biol. 2018 Oct 15;217(12):4124–40.

8. Matheny T, Rao BS, Parker R. Transcriptome-Wide Comparison of Stress Granules and P-Bodies Reveals that Translation Plays a Major Role in RNA Partitioning. Mol Cell Biol. 2019 Dec 15;39(24):612.

9. Bakheet T, Hitti E, Khabar KSA. ARED-Plus: an updated and expanded database of AU-rich element-containing mRNAs and pre-mRNAs. Nucleic Acids Research. 2018 Jan 4;46(D1):D218–20.

10. Hitti E, Bakheet T, Al-Souhibani N, Moghrabi W, Al-Yahya S, Al-Ghamdi M, et al. Systematic Analysis of AU-Rich Element Expression in Cancer Reveals Common Functional Clusters Regulated by Key RNA-Binding Proteins. Cancer Res. 2016 Jul 15;76(14):4068–80.

11. Blanco FF, Sanduja S, Deane NG, Blackshear PJ, Dixon DA. Transforming growth factor β regulates P-body formation through induction of the mRNA decay factor tristetraprolin. Mol Cell Biol. 2014 Jan;34(2):180–95.

12. Corcoran JA, Khaperskyy DA, Johnston BP, King CA, Cyr DP, Olsthoorn AV, et al. Kaposi's sarcoma-associated herpesvirus G-protein-coupled receptor prevents AU-rich-element-mediated mRNA decay. J Virol. 2012 Aug;86(16):8859–71.

13. Corcoran JA, Johnston BP, McCormick C. Viral Activation of MK2-hsp27-p115RhoGEF-RhoA Signaling Axis Causes Cytoskeletal Rearrangements, P-body Disruption and ARE-mRNA Stabilization. Robertson ES, editor. PLoS Pathogens. Public Library of Science; 2015 Jan 8;11(1):e1004597.

14. Franks TM, Lykke-Andersen J. TTP and BRF proteins nucleate processing body formation to silence mRNAs with AU-rich elements. Genes Dev. 2007 Mar 15;21(6):719–35.

15. Vindry C, Marnef A, Broomhead H, Twyffels L, Ozgur S, Stoecklin G, et al. Dual RNA Processing Roles of Pat1b via Cytoplasmic Lsm1-7 and Nuclear Lsm2-8 Complexes. CellReports. 2017 Aug 1;20(5):1187–200.

16. Corcoran JA, McCormick C. Viral activation of stress-regulated Rho-GTPase signaling pathway disrupts sites of mRNA degradation to influence cellular gene expression. Small GTPases. Taylor & Francis; 2015 Oct 2;6(4):178–85.

17. Standart N, Weil D. P-Bodies: Cytosolic Droplets for Coordinated mRNA Storage. Trends Genet. 2018 Aug;34(8):612–26.

18. Docena G, Rovedatti L, Kruidenier L, Fanning A, Leakey NAB, Knowles CH, et al. Down-regulation of p38 mitogen-activated protein kinase activation and proinflammatory cytokine production by mitogen-activated protein kinase inhibitors in inflammatory bowel disease. Clin Exp Immunol. John Wiley & Sons, Ltd; 2010 Oct;162(1):108–15.

19. Jangra RK, Yi M, Lemon SM. DDX6 (Rck/p54) is required for efficient hepatitis C virus replication but not for internal ribosome entry site-directed translation. J Virol. 2010 Jul;84(13):6810–24.

20. Ng CS, Kasumba DM, Fujita T, Luo H. Spatio-temporal characterization of the antiviral activity of the XRN1-DCP1/2 aggregation against cytoplasmic RNA viruses to prevent cell death. Cell Death & Differentiation. Nature Publishing Group; 2020 Feb 7;36:932–20.

21. Ostareck DH, Naarmann-de Vries IS, Ostareck-Lederer A. DDX6 and its orthologs as modulators of cellular and viral RNA expression. Wiley Interdiscip Rev RNA. 2014 Sep;5(5):659–78.

22. Dougherty JD, Tsai W-C, Lloyd RE. Multiple Poliovirus Proteins Repress Cytoplasmic RNA Granules. Viruses. Multidisciplinary Digital Publishing Institute; 2015 Nov 25;7(12):6127–40.

23. Dougherty JD, White JP, Lloyd RE. Poliovirus-mediated disruption of cytoplasmic processing bodies. J Virol. 2011 Jan;85(1):64–75.

24. Gaete-Argel A, Márquez CL, Barriga GP, Soto-Rifo R, Valiente-Echeverría F. Strategies for Success. Viral Infections and Membraneless Organelles. Front Cell Infect Microbiol. 2019;9:336.

607 25. McCormick C, Khaperskyy DA. Translation inhibition and stress granules in the antiviral
608 immune response. Nature Reviews Immunology. Nature Publishing Group; 2017
609 Oct;17(10):647–60.

610 26. Tsai W-C, Lloyd RE. Cytoplasmic RNA Granules and Viral Infection. Annu Rev Virol.
611 Annual Reviews; 2014 Nov;1(1):147–70.

612 27. Onomoto K, Jogi M, Yoo J-S, Narita R, Morimoto S, Takemura A, et al. Critical role of
613 an antiviral stress granule containing RIG-I and PKR in viral detection and innate
614 immunity. Kanai A, editor. PLoS ONE. Public Library of Science; 2012;7(8):e43031.

615 28. Abernathy E, Glaunsinger B. Emerging roles for RNA degradation in viral replication and
616 antiviral defense. Virology. 2015 May;479-480:600–8.

617 29. Núñez RD, Budt M, Saenger S, Paki K, Arnold U, Sadewasser A, et al. The RNA
618 Helicase DDX6 Associates with RIG-I to Augment Induction of Antiviral Signaling. Int J
619 Mol Sci. Multidisciplinary Digital Publishing Institute; 2018 Jun 26;19(7):1877.

620 30. Balinsky CA, Schmeisser H, Wells AI, Ganesan S, Jin T, Singh K, et al. IRAV
621 (FLJ11286), an Interferon-Stimulated Gene with Antiviral Activity against Dengue Virus,
622 Interacts with MOV10. Diamond MS, editor. J Virol. 2017 Mar 1;91(5):504.

623 31. Wang H, Chang L, Wang X, Su A, Feng C, Fu Y, et al. MOV10 interacts with Enterovirus
624 71 genomic 5'UTR and modulates viral replication. Biochem Biophys Res Commun. 2016
625 Oct 21;479(3):571–7.

626 32. Cuevas RA, Ghosh A, Wallerath C, Hornung V, Coyne CB, Sarkar SN. MOV10 Provides
627 Antiviral Activity against RNA Viruses by Enhancing RIG-I-MAVS-Independent IFN
628 Induction. J Immunol. 2016 May 1;196(9):3877–86.

629 33. Burdick R, Smith JL, Chaipan C, Friew Y, Chen J, Venkatachari NJ, et al. P body-
630 associated protein Mov10 inhibits HIV-1 replication at multiple stages. J Virol. 2010
631 Oct;84(19):10241–53.

632 34. Burgess HM, Mohr I. Cellular 5“-3” mRNA exonuclease Xrn1 controls double-stranded
633 RNA accumulation and anti-viral responses. Cell Host and Microbe. 2015 Mar
634 11;17(3):332–44.

635 35. Lumb JH, Li Q, Popov LM, Ding S, Keith MT, Merrill BD, et al. DDX6 Represses
636 Aberrant Activation of Interferon- Stimulated Genes. CellReports. ElsevierCompany;
637 2017 Jul 25;20(4):819–31.

638 36. Li Y, Chen R, Zhou Q, Xu Z, Li C, Wang S, et al. LSm14A is a processing body-
639 associated sensor of viral nucleic acids that initiates cellular antiviral response in the early
640 phase of viral infection. Proc Natl Acad Sci USA. 2012 Jul 17;109(29):11770–5.

37. V'kovski P, Kratzel A, Steiner S, Stalder H, Thiel V. Coronavirus biology and replication: implications for SARS-CoV-2. Nat Rev Microbiol. Nature Publishing Group; 2020 Oct 28;5:536–16.

38. Cui J, Li F, Shi Z-L. Origin and evolution of pathogenic coronaviruses. Springer US; 2019 Feb 6;:1–12.

39. Fielding CA, Jones GW, McLoughlin RM, McLeod L, Hammond VJ, Uceda J, et al. Interleukin-6 signaling drives fibrosis in unresolved inflammation. Immunity. 2014 Jan 16;40(1):40–50.

40. Blanco-Melo D, tenover BR. Imbalanced host response to SARS-CoV-2 drives development of COVID-19. Cell. 2020 Apr 15;:1–46.

41. Chen G, Wu D, Guo W, Cao Y, Huang D, Wang H, et al. Clinical and immunological features of severe and moderate coronavirus disease 2019. J Clin Invest. American Society for Clinical Investigation; 2020 May 1;130(5):2620–9.

42. Pedersen SF, Ho Y-C. SARS-CoV-2: a storm is raging. Journal of Clinical Investigation. 2020 Mar 23;130(5):2202–5.

43. Andersen KG, Rambaut A, Lipkin WI, Holmes EC, Garry RF. The proximal origin of SARS-CoV-2. Nature Medicine. 2020 Mar 17;26(4):450–2.

44. Zou L, Ruan F, Huang M, Liang L, Huang H, Hong Z, et al. SARS-CoV-2 Viral Load in Upper Respiratory Specimens of Infected Patients. N Engl J Med. Massachusetts Medical Society; 2020 Mar 19;382(12):1177–9.

45. Park A, Iwasaki A. Type I and Type III Interferons - Induction, Signaling, Evasion, and Application to Combat COVID-19. Cell Host and Microbe. 2020 Jun 10;27(6):870–8.

46. Bastard P, Rosen LB, Zhang Q, Michailidis E, Hoffmann H-H, Zhang Y, et al. Auto-antibodies against type I IFNs in patients with life-threatening COVID-19. Science. 2020 Sep 24;129:eabd4585.

47. Zhang Q, Bastard P, Liu Z, Le Pen J, Moncada-Velez M, Chen J, et al. Inborn errors of type I IFN immunity in patients with life-threatening COVID-19. Science. 2020 Sep 24;:eabd4570.

48. Ackermann M, Mentzer SJ, Kolb M, Jonigk D. Inflammation and Intussusceptive Angiogenesis in COVID-19: everything in and out of Flow. Eur Respir J. 2020 Oct 2;383:2003147.

49. Yuen C-K, Lam J-Y, Wong W-M, Mak L-F, Wang X, Chu H, et al. SARS-CoV-2 nsp13, nsp14, nsp15 and orf6 function as potent interferon antagonists. Emerging Microbes & Infections. Taylor & Francis; 2020 Dec;9(1):1418–28.

675 50. Miorin L, Kehrer T, Sanchez-Aparicio MT, Zhang K, Cohen P, Patel RS, et al. SARS-
676 CoV-2 Orf6 hijacks Nup98 to block STAT nuclear import and antagonize interferon
677 signaling. Proc Natl Acad Sci USA. 2020 Oct 23;5:202016650–11.

678 51. Li Y, Renner DM, Comar CE, Whelan JN, Reyes HM, Cardenas-Diaz FL, et al. SARS-
679 CoV-2 induces double-stranded RNA-mediated innate immune responses in respiratory
680 epithelial derived cells and cardiomyocytes. bioRxiv. 2020 Sep 25;67:4504.

681 52. Banerjee AK, Blanco MR, Bruce EA, Honson DD, Chen LM, Chow A, et al. SARS-CoV-
682 2 disrupts splicing, translation, and protein trafficking to suppress host defenses. Cell.
683 Elsevier Inc; 2020 Oct 7;:1–66.

684 53. Konno Y, Kimura I, Uriu K, Fukushi M, Irie T, Koyanagi Y, et al. SARS-CoV-2 ORF3b
685 Is a Potent Interferon Antagonist Whose Activity Is Increased by a Naturally Occurring
686 Elongation Variant. CellReports. 2020 Sep 22;32(12):108185.

687 54. Sola I, Galán C, Mateos-Gómez PA, Palacio L, Zuñiga S, Cruz JL, et al. The
688 polypyrimidine tract-binding protein affects coronavirus RNA accumulation levels and
689 relocalizes viral RNAs to novel cytoplasmic domains different from replication-
690 transcription sites. J Virol. 3rd ed. 2011 May;85(10):5136–49.

691 55. Raaben M, Groot Koerkamp MJA, Rottier PJM, de Haan CAM. Mouse hepatitis
692 coronavirus replication induces host translational shutoff and mRNA decay, with
693 concomitant formation of stress granules and processing bodies. Cellular Microbiology.
694 2007 Sep;9(9):2218–29.

695 56. Wang X, Chang L, Wang H, Su A, Wu Z. Dcp1a and GW182 Induce Distinct Cellular
696 Aggregates and Have Different Effects on microRNA Pathway. DNA and Cell Biology.
697 2017 Jul;36(7):565–70.

698 57. Gordon DE, Jang GM, Bouhaddou M, Xu J, Obernier K, O'Meara MJ, et al. A SARS-
699 CoV-2-Human Protein-Protein Interaction Map Reveals Drug Targets and Potential Drug-
700 Repurposing. 2020 Mar 22;579:265–45.

701 58. Castle EL, Douglas P, Rinker KD, Corcoran JA. Viral manipulation of a novel
702 mechanoresponsive signaling axis disassembles processing bodies. 2020 May
703 15;48(4):245–65.

704 59. Corcoran JA, Khaperskyy DA, McCormick C. Assays for monitoring viral manipulation
705 of host ARE-mRNA turnover. Methods. 2011 Oct;55(2):172–81.

706 60. Pons S, Fodil S, Azoulay E, Zafrani L. The vascular endothelium: the cornerstone of
707 organ dysfunction in severe SARS-CoV-2 infection. Crit Care. BioMed Central; 2020 Jun
708 16;24(1):353–8.

709 61. Varga Z, Flammer AJ, Steiger P, Haberecker M, Andermatt R, Zinkernagel AS, et al.
710 Endothelial cell infection and endotheliitis in COVID-19. Elsevier Ltd; 2020 Apr 17;:1–2.

62. Libby P, Lüscher T. COVID-19 is, in the end, an endothelial disease. Eur Heart J. 3rd ed. 2020 Sep 1;41(32):3038–44.

63. Lowenstein CJ, Solomon SD. Severe COVID-19 is a Microvascular Disease. Circulation. Lippincott Williams & Wilkins Hagerstown, MD; 2020 Sep 2;191:148.

64. Ramakrishnan MA. Determination of 50% endpoint titer using a simple formula. World J Virol. 2016 May 12;5(2):85–6.

65. Cong Y, Ulasli M, Schepers H, Mauthe M, V'kovski P, Kriegenburg F, et al. Nucleocapsid Protein Recruitment to Replication-Transcription Complexes Plays a Crucial Role in Coronaviral Life Cycle. Dutch RE, editor. J Virol. American Society for Microbiology Journals; 2020 Jan 31;94(4):181.

66. Lu S, Ye Q, Singh D, Villa E, Cleveland DW, Corbett KD. The SARS-CoV-2 Nucleocapsid phosphoprotein forms mutually exclusive condensates with RNA and the membrane-associated M protein. bioRxiv. 2020 Jul 31;18(6):479.

67. Cascarina SM, Ross ED. A proposed role for the SARS-CoV-2 nucleocapsid protein in the formation and regulation of biomolecular condensates. FASEB j. 2020 Jun 20;34(8):9832–42.

68. McBride R, van Zyl M, Fielding BC. The coronavirus nucleocapsid is a multifunctional protein. Viruses. Multidisciplinary Digital Publishing Institute; 2014 Aug 7;6(8):2991–3018.

69. Peng T-Y, Lee K-R, Tarn W-Y. Phosphorylation of the arginine/serine dipeptide-rich motif of the severe acute respiratory syndrome coronavirus nucleocapsid protein modulates its multimerization, translation inhibitory activity and cellular localization. FEBS J. John Wiley & Sons, Ltd; 2008 Aug;275(16):4152–63.

70. Gussow AB, Auslander N, Faure G, Wolf YI, Zhang F, Koonin EV. Genomic determinants of pathogenicity in SARS-CoV-2 and other human coronaviruses. Proc Natl Acad Sci USA. 2020 Jun 30;117(26):15193–9.

71. Verheije MH, Hagemeijer MC, Ulasli M, Reggiori F, Rottier PJM, Masters PS, et al. The coronavirus nucleocapsid protein is dynamically associated with the replication-transcription complexes. J Virol. 2010 Nov;84(21):11575–9.

72. Robson F, Khan KS, Le TK, Paris C, Demirbag S, Barfuss P, et al. Coronavirus RNA Proofreading: Molecular Basis and Therapeutic Targeting. Mol Cell. 2020 Sep 3;79(5):710–27.

73. Becares M, Pascual-Iglesias A, Nogales A, Sola I, Enjuanes L, Zuñiga S. Mutagenesis of Coronavirus nsp14 Reveals Its Potential Role in Modulation of the Innate Immune Response. Perlman S, editor. J Virol. 3rd ed. 2016 May 12;90(11):5399–414.

74. Rao S, Hoskins I, Garcia PD, Tonn T, Ozadam H, Cenik ES, et al. Genes with 5′ terminal oligopyrimidine tracts preferentially escape global suppression of translation by the SARS-CoV-2 NSP1 protein. 2020 Sep 13;48:D166–70.

75. Schubert K, Karousis ED, Jomaa A, Scaiola A, Echeverria B, Gurzeler L-A, et al. SARS-CoV-2 Nsp1 binds the ribosomal mRNA channel to inhibit translation. Springer US; 2020 Sep 4;:1–19.

76. Fung T, Liao Y, Liu D. Regulation of Stress Responses and Translational Control by Coronavirus. Viruses. 2016 Jul;8(7):184–15.

77. Gaglia MM, Covarrubias S, Wong W, Glaunsinger BA. A common strategy for host RNA degradation by divergent viruses. J Virol. 2012 Sep;86(17):9527–30.

78. Narayanan K, Huang C, Lokugamage K, Kamitani W, Ikegami T, Tseng C-TK, et al. Severe acute respiratory syndrome coronavirus nsp1 suppresses host gene expression, including that of type I interferon, in infected cells. J Virol. 2008 May;82(9):4471–9.

79. Khaperskyy DA, Schmaling S, Larkins-Ford J, McCormick C, Gaglia MM. Selective Degradation of Host RNA Polymerase II Transcripts by Influenza A Virus PA-X Host Shutoff Protein. Palese P, editor. PLoS Pathogens. 2016 Feb;12(2):e1005427.

80. Schaecher SR, Touchette E, Schriewer J, Buller RM, Pekosz A. Severe Acute Respiratory Syndrome Coronavirus Gene 7 Products Contribute to Virus-Induced Apoptosis. J Virol. 2007 Oct 15;81(20):11054–68.

81. Zhu X, Chen J, Tian L, Zhou Y, Xu S, Long S, et al. Porcine Deltacoronavirus nsp5 Cleaves DCP1A To Decrease Its Antiviral Activity. Gallagher T, editor. J Virol. American Society for Microbiology Journals; 2020 Jul 16;94(15):128.

82. Dougherty JD, Reineke LC, Lloyd RE. mRNA decapping enzyme 1a (Dcp1a)-induced translational arrest through protein kinase R (PKR) activation requires the N-terminal enabled vasodilator-stimulated protein homology 1 (EVH1) domain. J Biol Chem. 2014 Feb 14;289(7):3936–49.

83. Eulalio A, Behm-Ansmant I, Izaurralde E. P bodies: at the crossroads of post-transcriptional pathways. Nat Rev Mol Cell Biol. Nature Publishing Group; 2007 Jan;8(1):9–22.

84. Ayache J, Bénard M, Ernoult-Lange M, Minshall N, Standart N, Kress M, et al. P-body assembly requires DDX6 repression complexes rather than decay or Ataxin2/2L complexes. Matera AG, editor. Mol Biol Cell. The American Society for Cell Biology; 2015 Jul 15;26(14):2579–95.

85. Tenekeci U, Poppe M, Beuerlein K, Buro C, Müller H, Weiser H, et al. K63-Ubiquitylation and TRAF6 Pathways Regulate Mammalian P-Body Formation and mRNA Decapping. Mol Cell. 2016 Jun 16;62(6):943–57.

86. Sheth U, Parker R. Decapping and decay of messenger RNA occur in cytoplasmic processing bodies. Science. American Association for the Advancement of Science; 2003 May 2;300(5620):805–8.

87. Rzeczkowski K, Beuerlein K, Müller H, Dittrich-Breiholz O, Schneider H, Kettner-Buhrow D, et al. c-Jun N-terminal kinase phosphorylates DCP1a to control formation of P bodies. J Cell Biol. 2011 Aug 22;194(4):581–96.

88. Stoecklin G, Mayo T, Anderson P. ARE-mRNA degradation requires the 5"-3" decay pathway. EMBO Rep. 2006 Jan;7(1):72–7.

89. Gordon DE, Jang GM, Bouhaddou M, Xu J, Obernier K, O'Meara MJ, et al. A SARS-CoV-2-Human Protein-Protein Interaction Map Reveals Drug Targets and Potential Drug-Repurposing. 2020 Mar 22;579:265–45.

90. Johnston BP, Pringle ES, McCormick C. KSHV activates unfolded protein response sensors but suppresses downstream transcriptional responses to support lytic replication. Swaminathan S, editor. PLoS Pathogens. 2019 Dec;15(12):e1008185.

91. Kamentsky L, Jones TR, Fraser A, Bray M-A, Logan DJ, Madden KL, et al. Improved structure, function and compatibility for CellProfiler: modular high-throughput image analysis software. Bioinformatics. 2011 Apr 15;27(8):1179–80.

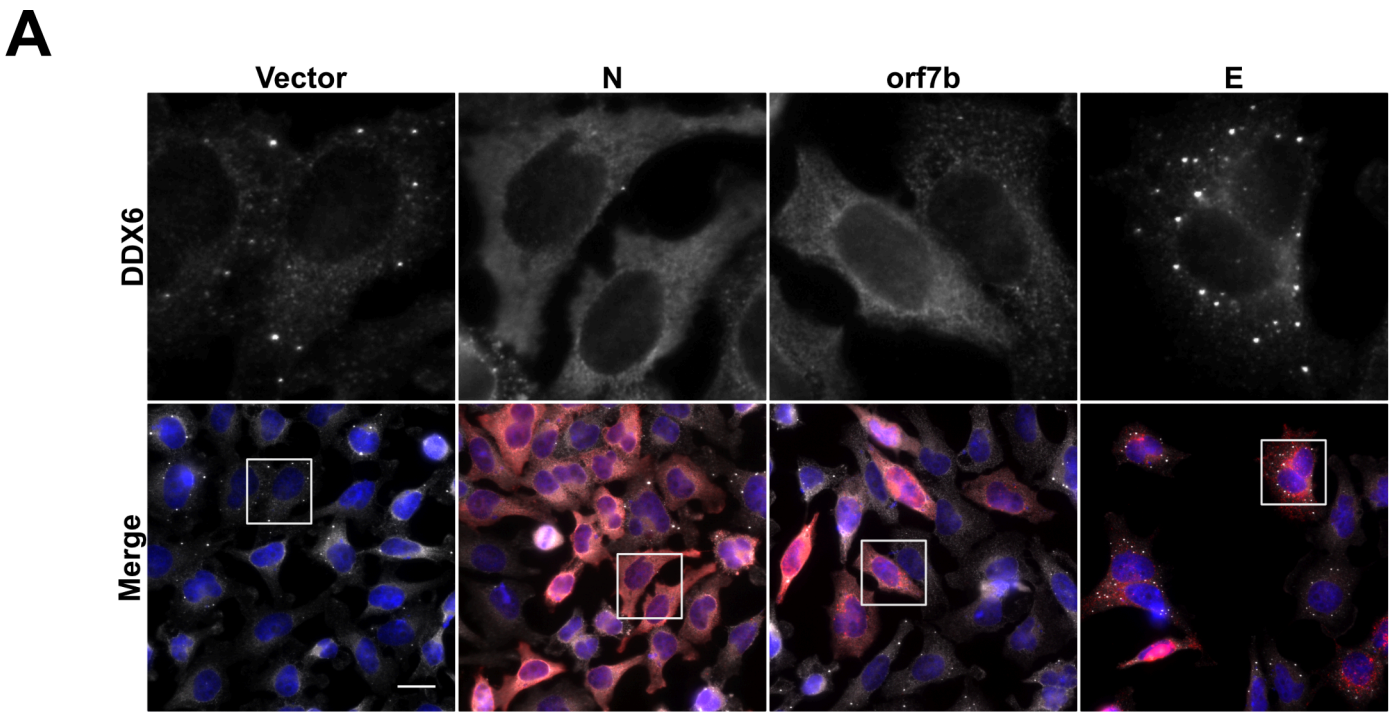

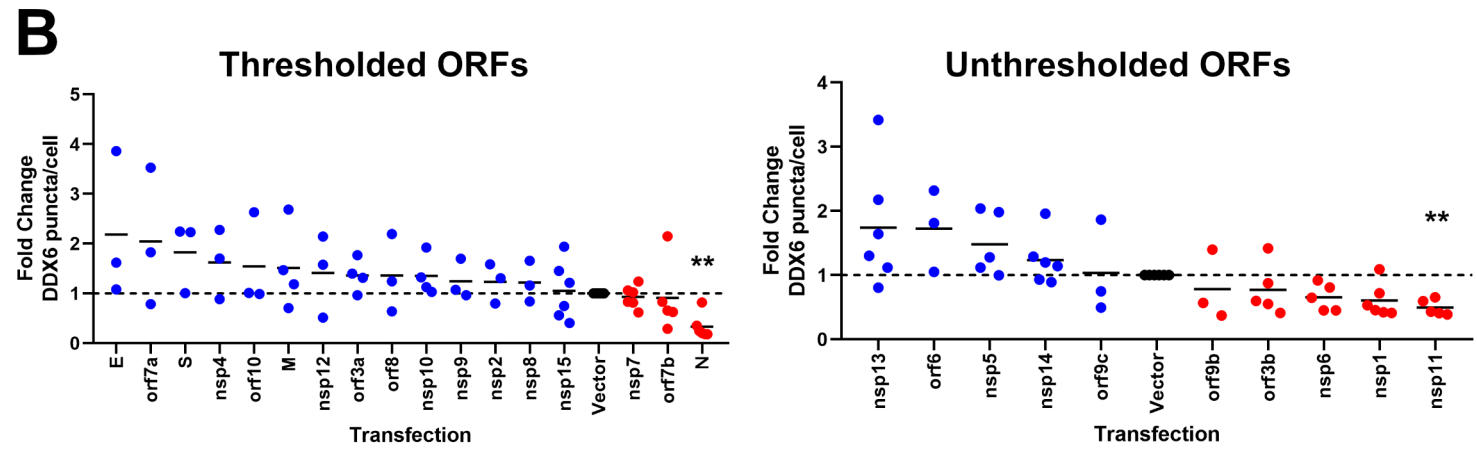

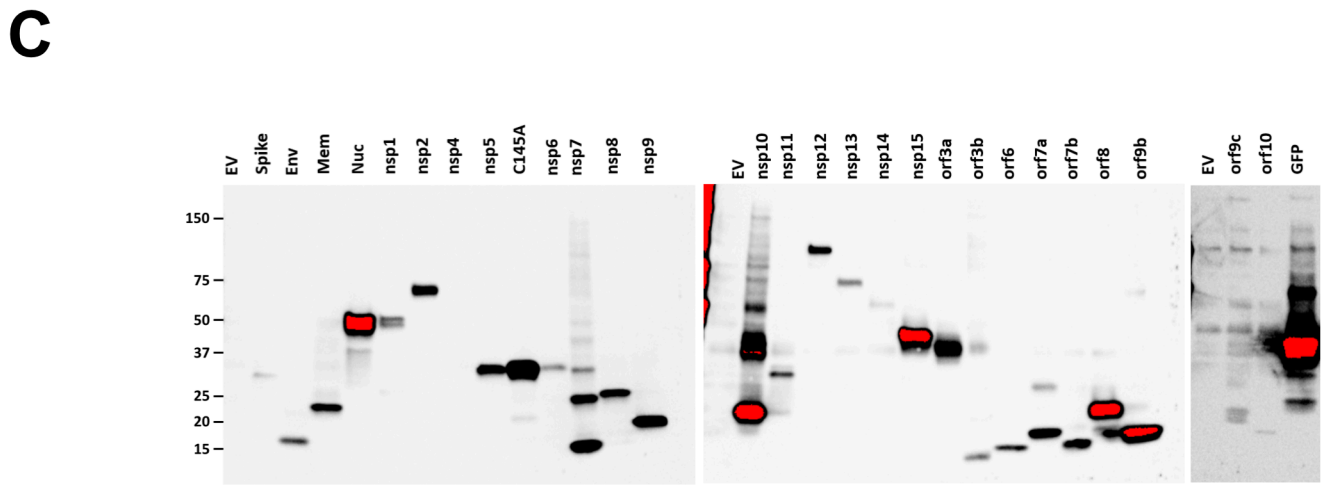

A

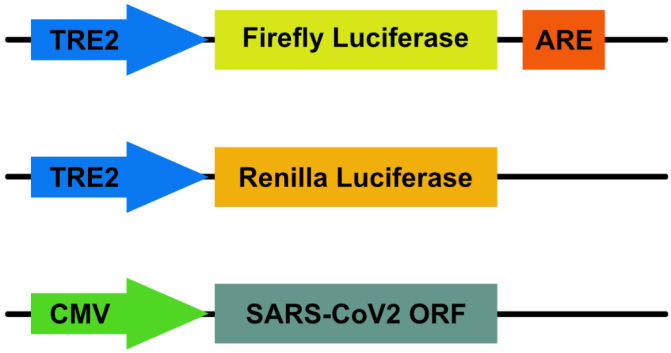

B

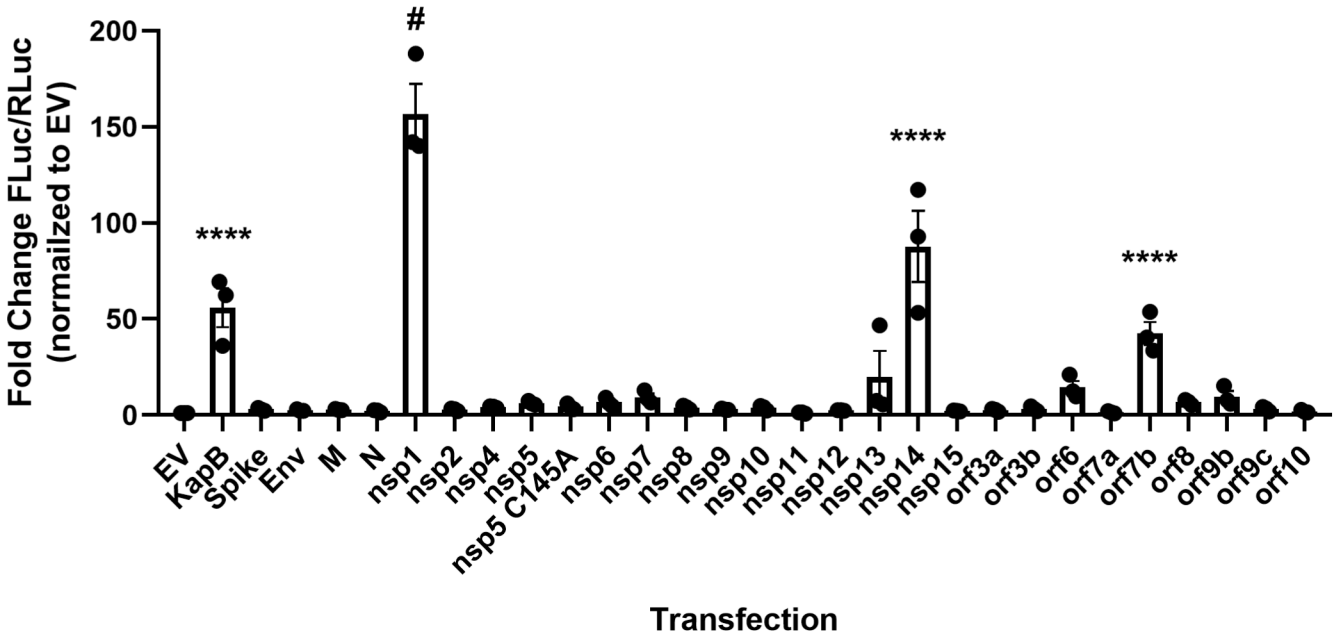

A

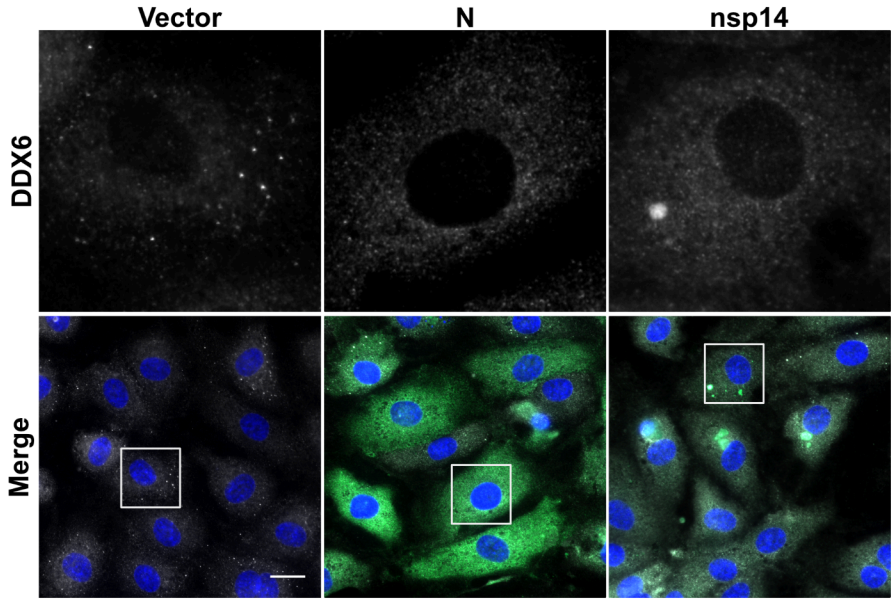

B

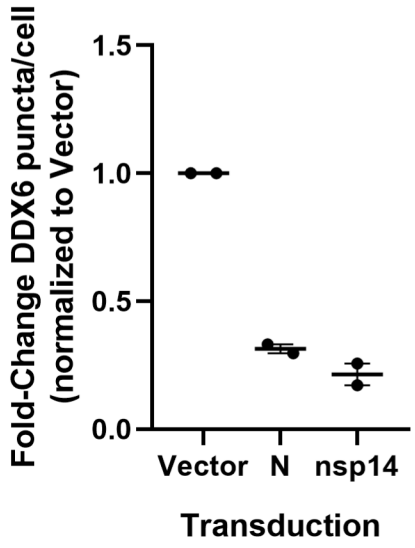

C

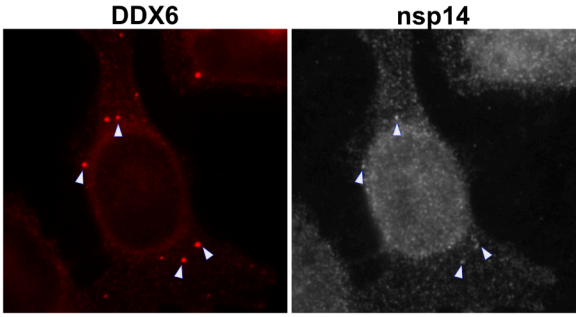

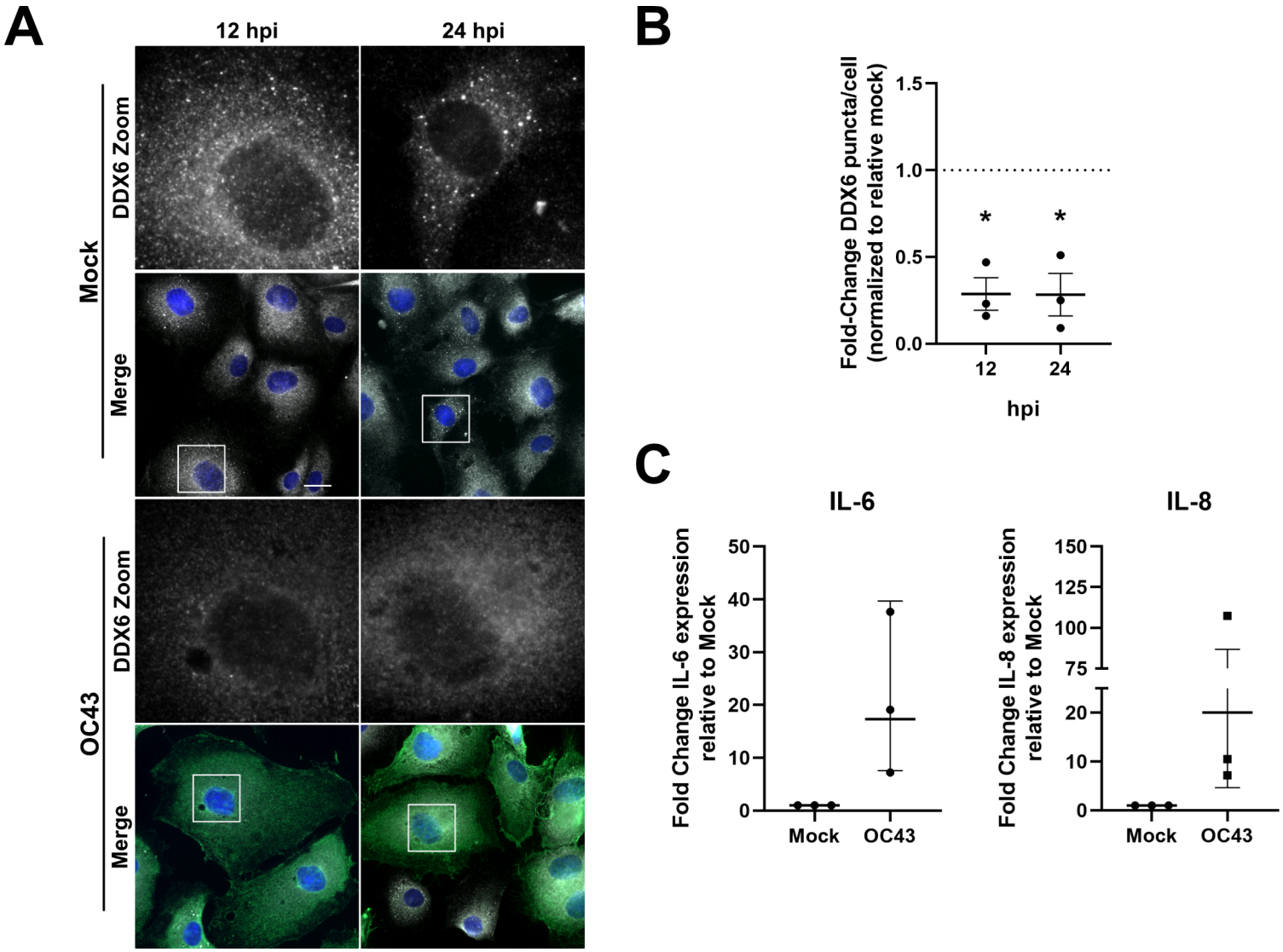

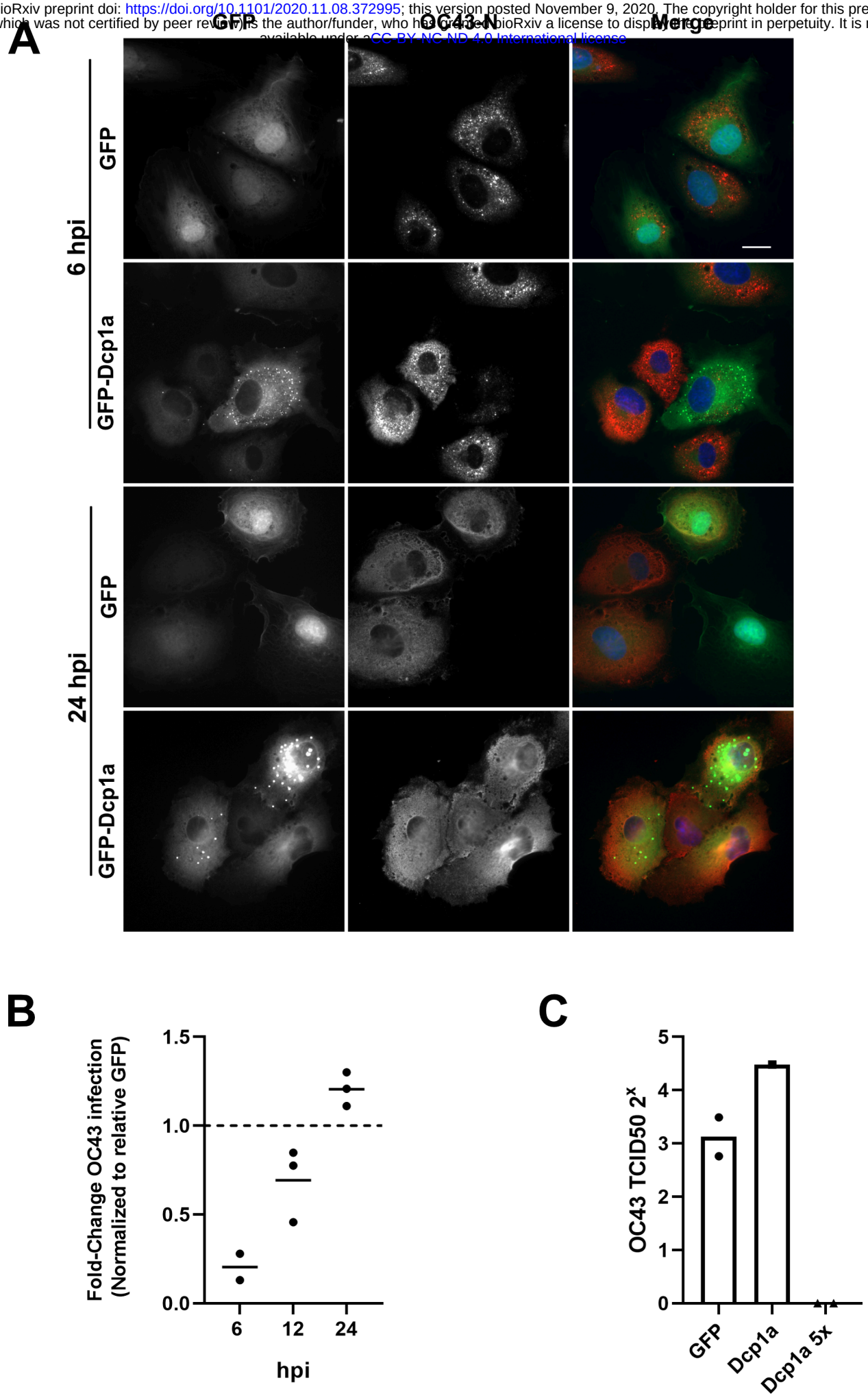

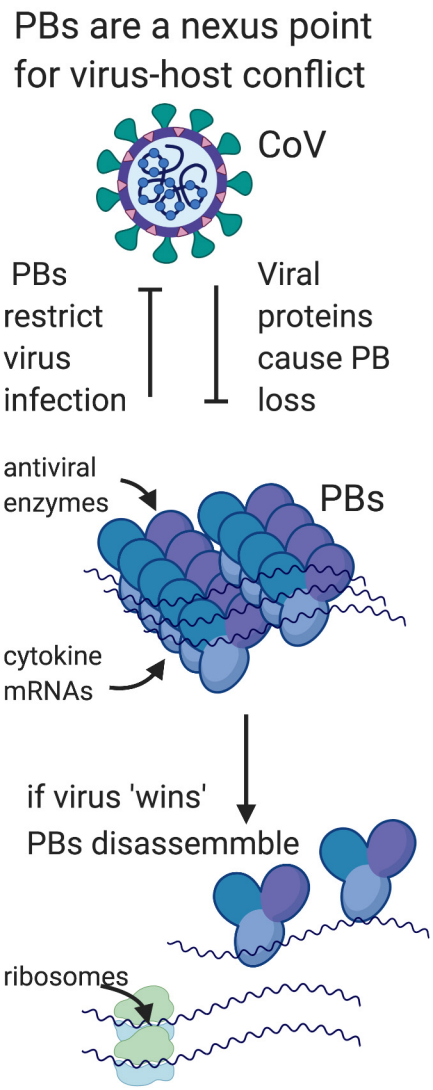

Repression of cytokine mRNA is relieved. This is an infected cell's call for reinforcements.